

# ***p*-type CuBr films with high hole conductivity and realization of *p*-CuBr/*n*-Si heterojunction solar cell**

K.V. Rajani <sup>a,b\*</sup>, S. Daniels<sup>a,b</sup>, M. Rahman<sup>c</sup>, A. Cowley<sup>a,b</sup> and P. J. McNally<sup>a</sup>

<sup>a</sup>*School of Electronic Engineering and <sup>b</sup>NCPST, Dublin City University, Dublin 9, Ireland*

<sup>c</sup>*SolarPrint Ltd., Ballymoss Road, Sandyford, Dublin 18, Ireland.*

## **ABSTRACT**

We present details of the deposition of transparent and earth-abundant *p*-type CuBr films with high hole conductivity and the fabrication and characterization of a prototype solar cell based on *p*-CuBr/*n*-Si heterojunctions. *p*-type CuBr films with typical resistivities and hole concentrations of  $7 \times 10^{-1} \Omega \text{cm}$  and  $7.5 \times 10^{19} \text{cm}^{-3}$ , respectively, are deposited by thermal evaporation followed by oxygen plasma treatment. The transparent *p*-type films show strong room temperature photoluminescence at  $\sim 2.97 \text{ eV}$ . The current voltage (*I*-*V*) characteristics of the heterojunctions show good diode behaviour. Power conversion efficiency of  $\sim 2 \%$  was achieved for the heterojunction device without any optimization of the cell structure under AM 1.5 illumination condition with a short circuit current ( $J_{sc}$ ) and open circuit voltage ( $V_{oc}$ ) of  $13.2 \text{ mA/cm}^2$  and  $0.44 \text{ V}$ , respectively.

Keywords: solar energy materials, semiconductors, thin films, CuBr

\* Corresponding author. e-mail: [rajani.vijayaraghavan@dcu.ie](mailto:rajani.vijayaraghavan@dcu.ie)

## **1. Introduction**

Heterojunction solar cell structures fabricated via simple and direct deposition of wide band gap transparent conducting thin films on Si substrate are reported [1] to have high power conversion efficiencies with their optimized configurations [2-4]. Efficiencies of around 10 % and  $\sim 4\%$ , respectively, are reported for ITO/Si and Al and Y co-doped ZnO/Si heterojunctions [2,4]. Although ITO based structures show high conversion efficiencies, they suffer from higher cost and scarcity of In raw material. Copper (I) bromide (CuBr) is an earth abundant I-VII inorganic semiconductor material with great potential for short-wavelength applications due to its large excitonic binding energy ( $\sim 108 \text{ meV}$ ) and direct band gap ( $\sim 3.1 \text{ eV}$  at 300 K) [5]. It exhibits good transparency ( $>80\%$ ) throughout the major portion of the visible region (above 420 nm) and shows strong absorption in the UV-violet region of the spectrum [6]. There are numerous reports on the huge potential of this material for excitonic and non-linear optical applications [6-8]. However, there are relatively few reports on the

semiconducting properties of CuBr [9-11]. The poor hole conductivity of as-deposited (ASD) CuBr represents a major limitation on the use of these materials. Hence the deposition of good quality CuBr films with highly improved *p*-type conductivity is extremely important for the future applications of this material system. Wide band gap CuBr with high *p*-type conductivity could be promising to use as hole conductor for the fabrication of solid-state dye sensitised solar cells [12]. In addition to this, the use of *p*-CuBr as a heterojunction partner for solar cells would help in better utilization of the UV-violet region of the solar spectrum. Similarly, this material would also be suitable for the realization of transparent *p-n* junction devices, such as thin film transistors, flat panel displays, and light emitting diodes [13-14].

CuBr is naturally a *p*-type material, with the *p*-type conductivity originating either from copper deficiency ( $\text{Cu}_{1-\delta}\text{Br}$ ) or via doping with oxygen [9]. The semiconducting properties of polycrystalline CuBr have been investigated by Knauth *et al.* using Hall effect, capacitive measurements and Mott-Schottky analysis [11]. According to their studies, oxygen impurities can increase the hole concentration and hence can act as effective acceptors for CuBr. Here we report the realization of *p*-CuBr/*n*-Si based *p-n* heterojunction devices and their photovoltaic properties for the first time by the deposition of *p*-type CuBr on a single crystal *n*-type Si wafer. The finding opens up the possibility of using novel, high *p*-type conducting and earth-abundant CuBr materials as transparent conducting, thin film heterojunction partners for solar cells.

## 2. Experimental

CuBr thin films of thickness  $400 \pm 10$  nm were deposited by the thermal evaporation of CuBr powder (99.999%) onto *n*-Si (111) and glass substrates (Edwards 306A vacuum evaporator). Prior to deposition the substrates were HF-cleaned to remove native  $\text{SiO}_2$  layer. An Ohmic contact (Al) was deposited on the back side of Si. The ASD CuBr samples are transferred immediately to a plasma chamber (Oxford Plasmalab 80 Plus-RIE), in which a mixture of  $\text{O}_2$  and Ar (4:1) is used as the working gas (RF power-300 W and pressure- $6.6 \times 10^{-2}$  mbar).

X-Ray diffraction (XRD) analysis was carried out (Bruker D8,  $\theta$ - $2\theta$  configuration) to determine the crystal structure of the CuBr films. The optical properties like absorption (Perkin Elmer Lambda 40 UV/Vis) and photoluminescence (PL) (J Y-Horiba LabRam) of the films were investigated. The electrical properties are measured using a Hall measurement (HL 5500 PC) set-up in the van der Pauw configuration in which CuBr/glass samples with gold ohmic contacts are used. The current-voltage (*I-V*) characteristics of the CuBr/Si heterojunction were examined (Keithley 4200 semiconductor parameter analyser). The photoresponse properties were measured (Newport Oriel solar simulator, AM1.5G,  $100 \text{ mW/cm}^2$ ).

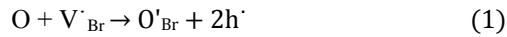
### 3. Results and discussion

The CuBr films deposited on glass substrates are exposed to oxygen plasma for 1, 3 and 5 min duration. The results of the Hall measurements are exemplified in table 1. The ASD films were highly resistive and could not be measured due to the poor ohmic contact of this film. The high resistivity of the ASD film is reduced by orders of magnitude as a result of oxygen plasma exposure. The resistivities ( $\rho$ ) and hole mobilities ( $\mu$ ) decrease from  $\sim 1.55$  to  $\sim 0.7$   $\Omega\text{cm}$  and  $\sim 0.45$  to  $\sim 0.24$   $\text{cm}^2\text{V}^{-1}\text{s}^{-1}$ , respectively, when the plasma exposure time increases from 1-3 min and thereafter increases to  $\sim 2.8$   $\Omega\text{cm}$  and  $0.65$   $\text{cm}^2\text{V}^{-1}\text{s}^{-1}$ , respectively, when the exposure time increases to 5 min. The hole concentration ( $N_h$ ) increases from  $\sim 8.5 \times 10^{18}$  to  $\sim 7.5 \times 10^{19}$   $\text{cm}^{-3}$  and then reduces to  $\sim 4 \times 10^{18}$   $\text{cm}^{-3}$  for exposure times of 1, 3 and 5 min, respectively.

**Table 1** Hall measurement results of  $p$ -CuBr films exposed to oxygen plasma for various time intervals.

Oxygen exposure time (min)	Resistivity ( $\Omega\text{cm}$ )	Hall mobility ( $\text{cm}^2\text{V}^{-1}\text{s}^{-1}$ )	Carrier density ( $\text{cm}^{-3}$ )
1	1.55	0.45	$8.5 \times 10^{18}$
3	0.7	0.245	$7.5 \times 10^{19}$
5	2.8	0.65	$4 \times 10^{18}$

One of the possible mechanisms behind the higher  $N_h$  in the oxygen plasma treated (PT) samples could be the introduction of substitutional oxygen onto bromine sites, thereby creating acceptor levels in the lattice, in addition to the contribution from the copper deficiencies already present in the samples. The possible mechanism of doping can be described using the Kröger-Vink notation as follows [9]:



where  $V_{\text{Br}}$ ,  $\text{O}'_{\text{Br}}$  and  $h^{\cdot}$  are the vacancy in the Br site with a single positive charge, oxygen in the Br site with an apparent negative charge and a hole, respectively. The increase in  $N_h$  and reduction in  $\rho$  with the increase of plasma exposure time from 1-3 min could be attributed to the presence of relatively higher number of oxygen species in the samples and hence the higher number of acceptor levels. The further decrease in  $N_h$  (or increase in  $\rho$ ) associated with the higher exposure time (5 min) could be due to the fact that some of the incorporated oxygen will occupy the plasma created defects and simply act as a defect passivation layer rather than contributing to the conduction process (the presence of increased defects in the PT films are verified by AFM, attached in

supplementary materials). The slight improvement in the mobility of the 5 min PT film would be due to small increases in the grain size of this film (confirmed from AFM and XRD measurements), which would reduce the probability of grain boundary scattering. The higher the plasma exposure time the more the possibility of etching and formation of defects or damage caused by the energetic ion bombardment on the film. Hence, only the 1 min PT films are used for the *p-n* device fabrication.

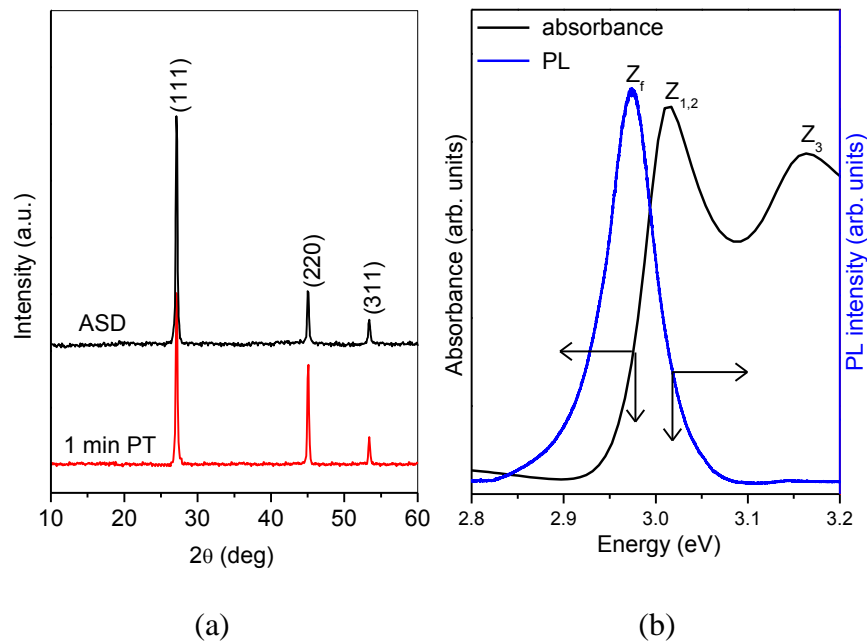


**Fig.1.**(a) XRD pattern of the ASD and 1 min PT CuBr films deposited on Si (111) substrate and (b) room temperature PL and absorbance spectrum of a typical 1 min PT CuBr film.

Figure 1(a) indicates the XRD pattern of ASD and the 1 min PT films. The XRD patterns indicate the presence of (111), (220) and (311) reflections of polycrystalline, zinc-blende CuBr with preferential orientation along the (111) direction. There is no significant structural variation of the CuBr films observed as a result of oxygen plasma treatment. Figure 1(b) illustrates room temperature PL and absorbance spectrum of 1 min PT CuBr film. The spectrum indicates a strong emission at around 2.97 eV (~417 nm), originating from the  $Z_f$  free exciton, which is in good agreement with previous reports on the room temperature PL of the ASD CuBr films [6,15]. The FWHM of the PL peak obtained using a Gaussian fit was nearly 8.5 nm, which emphasizes the good optical quality of the *p*-CuBr film. The absorption spectrum shows two main absorption peaks around 3.01 eV (~411 nm) and 3.17 eV (~391 nm) which are due to the  $Z_{1,2}$  and  $Z_3$  excitons of CuBr, respectively [16].

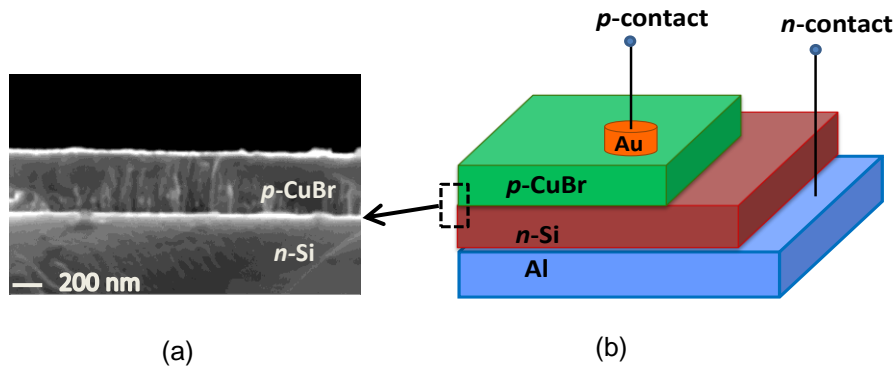


**Fig.2.** (a) SEM image of the cross-sectional view of the  $n$ -Si/ $p$ -CuBr heterojunction interface and (b) schematic configuration of the  $p$ - $n$  heterojunction device.

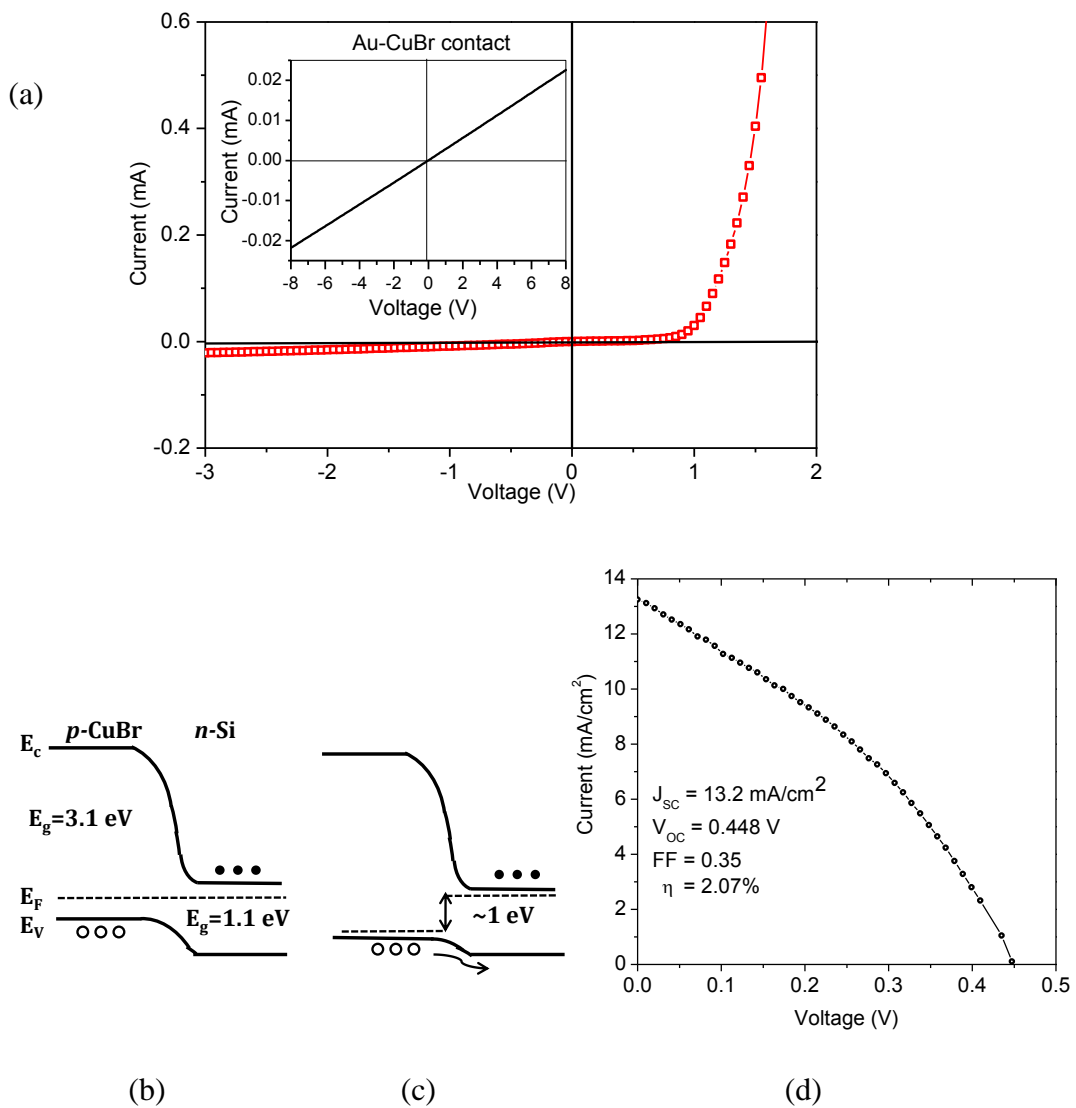


**Fig. 3.** (a)  $I$ - $V$  characteristics of the  $p$ -CuBr/ $n$ -Si heterojunction measured in the dark.  $I$ - $V$  curve of Au-CuBr contact (Inset top left), Schematic of the band diagram of the  $p$ -CuBr/ $n$ -Si heterojunction diode at (b) thermal equilibrium and (c) under forward bias, (d)  $J$ - $V$  characteristics of  $p$ -CuBr/ $n$ -Si heterojunction

Figure 2 (a) and (b) respectively indicate the SEM image of the cross-sectional view of the *n*-Si/*p*-CuBr heterojunction interface and the schematic configuration of the *p*-*n* heterojunction device. The *I*-*V* characteristics of the heterojunction (dark) are illustrated in figure 3 (a). A linear Au-CuBr *I*-*V* curve (inset top left) confirms the ohmic nature of the top contact. The *n*-Si/*p*-CuBr junction *I*-*V* curve exhibits good rectifying behaviour with a rectification ratio of  $I_F/I_R \sim 31$  at 3 V, where  $I_F$  and  $I_R$  are the forward and reverse currents, respectively, indicating the formation of a *p*-*n* diode. The reverse leakage current and the turn on voltage of the diode are  $2 \times 10^{-5}$  A at 3 V and  $\sim 1$  V, respectively. The ideality factor of the diode is calculated to be  $n \sim 2.2$ , indicates that the conduction is dominated by non-thermionic processes [17]. The higher value of  $n$  could be attributed to the presence of higher recombination currents in the depletion region or to the interface defect states. The lower turn-on voltage ( $\sim 1$  V) can be explained using a schematic band structure of the heterojunction (Figure 3 (b) & (c)). As the the band gap energy ( $E_g$ ) of the *p*-CuBr is more than twice that of the *n*-Si and the carrier concentration in the *p*-region is orders of magnitude  $>$  that of the *n*-region, the energy barrier for holes will be thinner than that for electrons in the heterojunction interface. As a forward bias is applied to the heterojunction, the valence band (VB) maximum of Si shifts to a higher energy level and approaches the VB edge of *p*-CuBr, and the barrier to hole transport decreases. Thus the application of forward bias of the order of 1 V leads to the transport of holes from the VB of CuBr to the VB of Si and produces conduction current. The current density-voltage (*J*-*V*) characteristics of a typical illuminated heterojunction are presented in Figure 3 (d). The heterojunction exhibits good rectification in the presence of light too. When the heterojunction is illuminated, photons with energy ( $E$ ) greater than the  $E_g$  of CuBr will be absorbed by the film and those with energy  $E < E_g$  will be transmitted through the film and absorbed by the underlying Si substrate and *e*-*h* pair generation takes place in both the layers and the current increases as the reverse bias increases. The power conversion efficiency of the solar cell can be expressed as  $\eta = (J_{sc} \times V_{oc} \times FF) \times 100 / P_i$ , where  $P_i$  is the intensity of the incident light,  $J_{sc}$  is the short circuit current,  $V_{oc}$  is the open circuit voltage and  $FF$  is the fill factor. The performance of the device is examined using the values of the parameters extracted from the *J*-*V* plot as  $J_{sc} = 13.2$  mA/cm<sup>2</sup>,  $V_{oc} = 0.448$  V,  $FF = 0.35$  giving a power conversion efficiency ( $\eta$ ) of 2.07%. We have tested various devices prepared under same experimental conditions and configuration and achieved an average efficiency of  $\sim 2\%$  without any optimization of the device structure.

Since the present report shows substantial room for the improvement in all key cell parameters, further process optimization and development is necessary. However, the initial results on the proof-of concept device demonstrate the great potential of *p*-CuBr for the solar cell and short-wavelength applications and the next stage will be the optimization of the solar cell structure to get maximum efficiency out of that.

#### 4. Conclusion

In conclusion, *p*-type CuBr thin films with good violet emission were grown on *n*-Si substrates by vacuum evaporation of CuBr powder followed by oxygen plasma treatment. Hall measurements confirm the good *p*-type behaviour of the films with a resistivity and hole concentration of 1.55  $\Omega\text{cm}$  and  $8.5 \times 10^{18} \text{ cm}^{-3}$ , respectively, for a 1 min PT CuBr film. A *p*-CuBr/*n*-Si heterojunction device was fabricated and its rectifying properties were verified for the first time. The power conversion efficiency was  $\sim 2.07\%$  without any optimization of the device structure. This report may lead to the possibility of using the transparent and low-cost CuBr material system for solar cell and short-wavelength light applications.

#### Acknowledgments

We acknowledge the support of SFI's 06/RFP/ENE/027 and EI's CFTD/07/IT/331. This work was also part-funded by the Irish Higher Education Authority PRTL "INSPIRE" project, SFI's Strategic Research Cluster Programme ("Precision" 08/SRC/I1411), and the ENIAC (EU and Enterprise Ireland).

#### References

- [1] Kim J, Yun JH, Park YC, Anderson WA. *Mater Lett* 2012;75:99.
- [2] Hsu FH, Wang NF, Tsai YZ, Houg MP. *Solar Energy* 2012; 86:3146.
- [3] Kobayashi H, Kogetsu Y, Ishida T, Nakato Y. *J Appl Phys* 1993;74: 4756.
- [4] Manificier JC, Szepessy L. *Appl Phys Lett* 1977;31:459.
- [5] Brinkman WF, Rice TM, Bell B. *Phys Rev B* 1973;8:1570.
- [6] Kondo S, Saito T. *Appl Phys Lett* 2007;90: 201915.
- [7] Li H, Liu R, Kang H, Zheng Y, Xu Z. *Electrochim Acta* 2008;54:242.
- [8] Kondo S, Ohsawa H, Asada H, Saito T. *J Appl Phys* 2010;107:103526.
- [9] Knauth, P, Massiani Y, Pasquinelli M. *Phys Stat Sol (a)* 1998;165:461.
- [10] Nanda KK, Kruis FE, Fissan H, Behera SN. *J Appl Phys* 2004;95:5035.
- [11] Knauth P, Massiani Y. *J. Electroanal. Chem.* 1998;442:229.
- [12] Li B, Wang L, Kang B, Wang P, Qiu Y. *Solar Energy Mater Solar Cells* 2006;90:549.
- [13] Fortunato E, Barquinha P, Martins R *Adv Mater* 2012;24:2945.
- [14] Kawazoe H, Yasukawa M, Hyodo H, Kurita M, Yanagi H, Hosono H. *Nature* 1997;389:939.
- [15] Nakayama M, Soumura A, Hamasaki K, Takeuchi H, Nishimura H. *Phys Rev B* 1997;55:10099.
- [16] Cardona M. *J Phys Chem Sol* 1963;24:1543.

[17] Alivov YI, Özgür Ü, Dogan S, Johnstone D, Avrutin V, Onojima, N, et al. Appl Phys Lett  
2005;86:241108.